NASA TECHNICAL TRANSLATION NASA TT F-16,141

AERODYNAMIC DESIGN OF AIRFOIL SECTIONS

K. Uemaya, M. Ōmura, and T. Tanioka

Translation of "Nijigen yokukei no kūriki sekkeihō," Mitsubishi Juko Giho, Vol. 11, No. 2, 1974, pp. 1-12

NATIONAL AERONAUTICS AND SPACE ADMINISTRATION
WASHINGTON, D.C. 20546 FEBRUARY 1975

AERODYNAMIC DESIGN OF AIRFOIL SECTIONS

K. Uemaya, M. Ōmura, and T. Tanioka,
Aerodynamic Research Section, 1st Technical Division,
Nagoya Aircraft Manufacturing Plant (Mitsubishi Heavy Industries)

1. Introduction

/1*

In the area of research on airfoil sections, which have a very important effect on aircraft performance, fragmentary studies conducted in Great Britain and prewar Germany were followed by a large-scale systematic airfoil research and development project undertaken by NACA of the United States. These NACA airfoil sections have been widely used in aircraft of all types from low-speed aircraft to supersonic aircraft. But we have now reached a stage where it has become possible to develop airfoil sections which meet the various aircraft performance requirements more rationally thanks to a deeper understanding of the effects of the boundary layer and compressibility, as well as to progress in the area of computers.

After a look at the history of the research and development of past airfoil sections, this report will discuss methods for designing optimal airfoil sections to satisfy required specifications for the speed range from low speed to high subsonic speeds, and present their design applications in the form of two new types of airfoil sections and cascade blades. This report will mention calculation examples, most of which have been presented in various publications, but many of the calculations methods cited in this text have already been programmed at the Nagoya Aircraft Manufacturing Plant and are being used in the designing of such airfoil sections as the rooftop-rear-loading airfoils (see

---

* Numbers in the margin indicate pagination in the foreign text.

Section 7.2). As far as aircraft wings are concerned, there are various important subjects which we are exploring, such as transonic airfoils, which include supercritical airfoils that are rapidly gaining attention these days, and sectional designs of three-dimensional wings. These subjects will be dealt with on other occasions, while this report will deal solely with two-dimensional subsonic airfoil sections (under the velocity of sound at every point on the wing surface).

2. History of Airfoil Research and Development

In the early days, airfoils used to consist of cambered flat sheets, but when practical applications of the thin wing theory became feasible, there began the designing of airfoils which were thin wings appropriately thickened to decrease the travel of the center of pressure. The Göttingen airfoils (Fig. 1) were developed in Germany in the 1920's, while in the United States the NACA four-digit airfoils (Fig. 2) were designed in the early 1930's. Shortly thereafter, in the United States, airfoils of high maximum lift coefficient C_{Lmax} and low minimum drag coefficient C_{D0}, called the NACA five-digit airfoils (Fig. 3A), were developed and were widely used in various countries before the war, especially the NACA 23102. /2

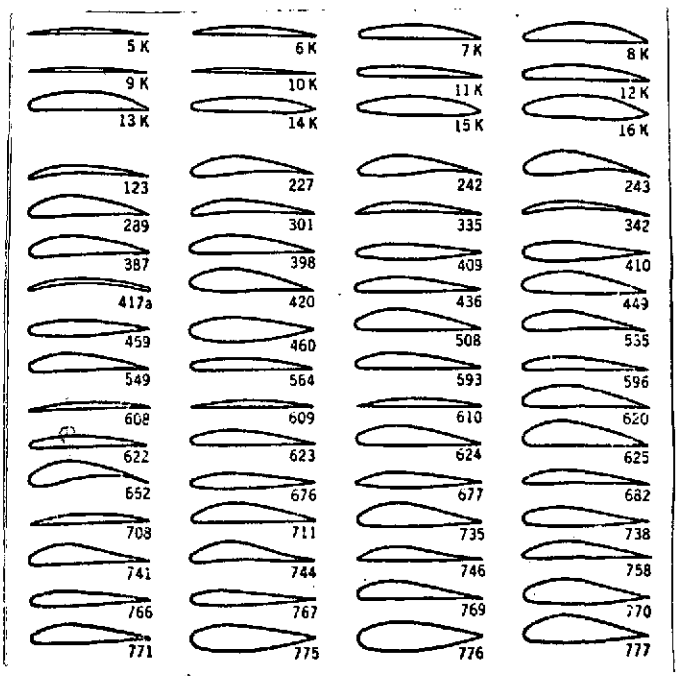

Fig. 1. Some of the Göttingen airfoils.

These NACA profile sections were designed by systematically varying the distributions of the profile thickness or camber. Rather than being designed with clear

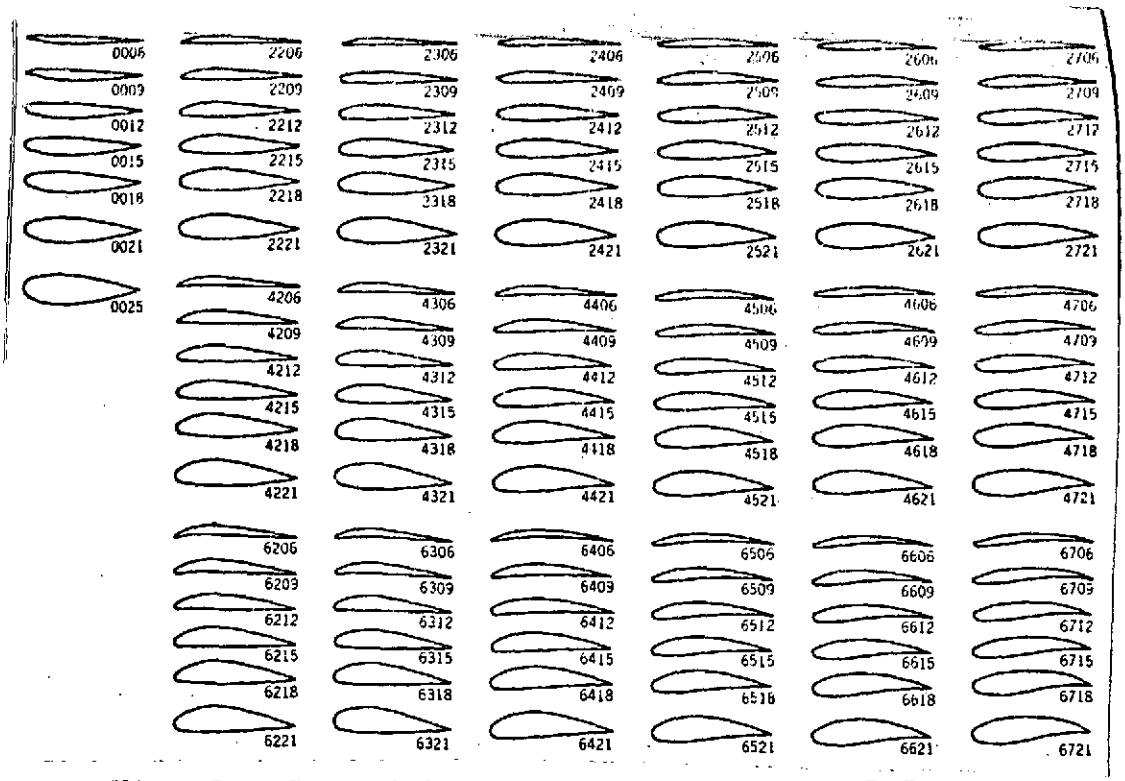

Fig. 2. Some NACA four-digit airfoils [1].

targets in terms of aerodynamic characteristics, they were built for the purpose of selecting those of superior characteristics and defining areas of possible improvements through wind tunnel tests.

Meanwhile, a method for calculating the pressure distribution around a given airfoil section in a nonviscous, imcompressible flow was developed for the first time in the early 1930's [3]. Then, in the early 1940's, it became possible to construct airfoils possessing given pressure distributions by means of approximation [4]. Also, due to progress in research on the boundary layer, it became possible to estimate the point of transition from laminar flow to turbulent flow, so that for the first time the pressure distribution on the wing became an important factor in airfoil design. Consequently, there occurred a shift from the previous concept of selecting airfoils of good characteristics by systematically varying their shapes to the approach of attempting to

/3

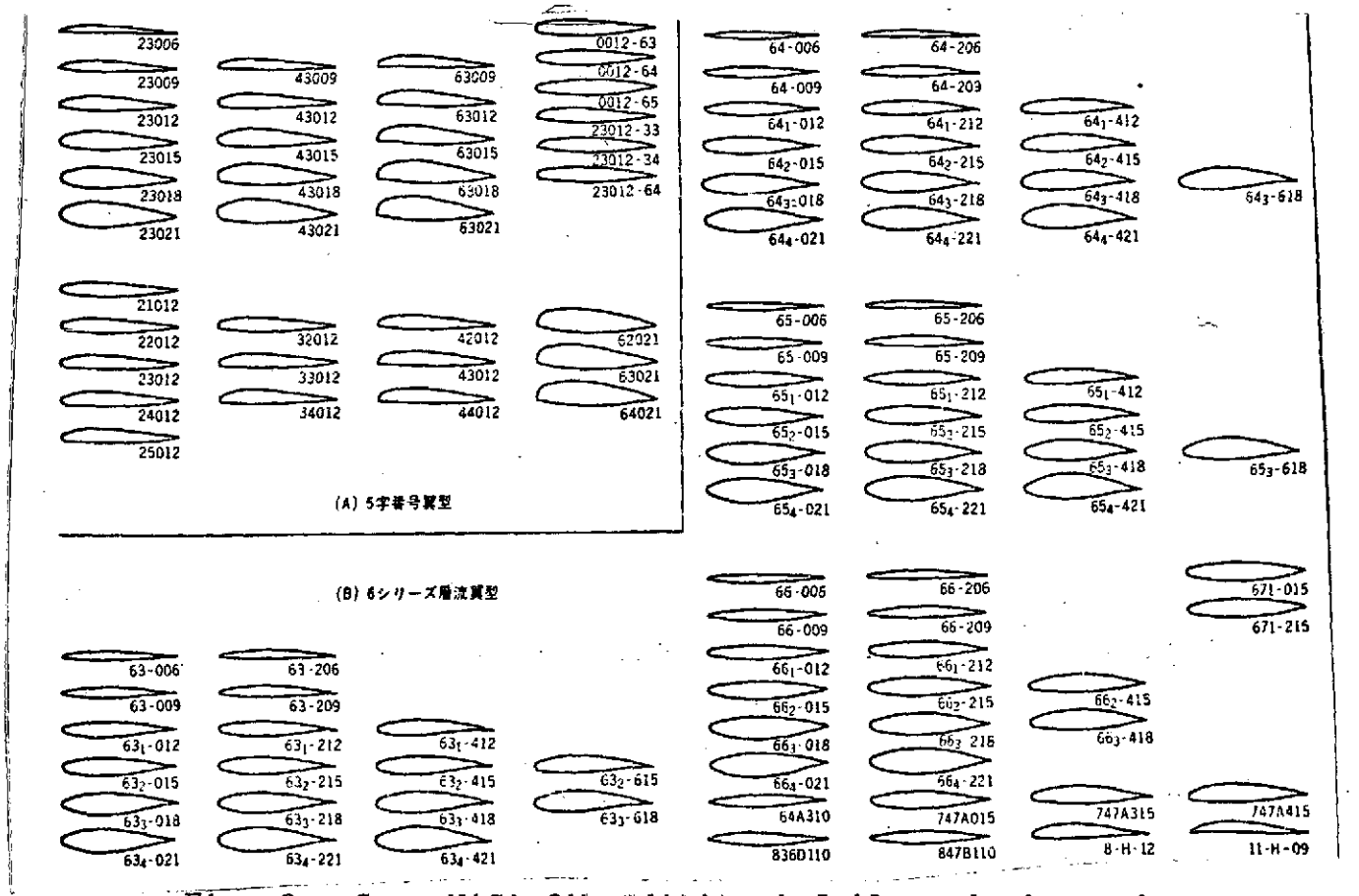

Fig. 3. Some NACA five-digit airfoils and six-series laminar airfoils [1].
(A) five-digit airfoils
(B) six-series laminar flow airfoils

design practical airfoil sections by systematically varying their pressure distribution.

As a result, the first laminar flow airfoils, the NACA one-series airfoils, were developed in the late 1930's. In this series, system 16 was widely used in propellers. This series was followed by the development of the two-series to five-series laminar flow airfoils, in which the drag against the design lift was greatly reduced, but the problem of low maximum lift due to the small curvature of the wing still remained. This problem was successfully solved by the six-series laminar flow airfoils (Fig. 3B), which found wide application both before and after the war.

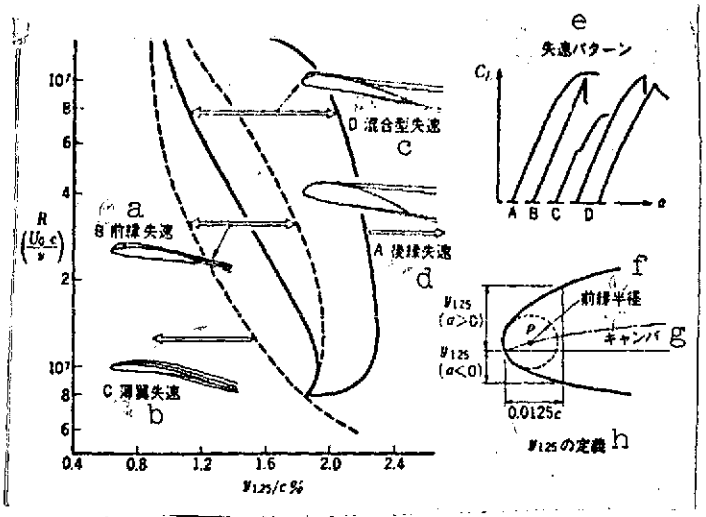

Fig. 4. Relationship between nose shape and stall characteristics [6].

Key: a. Nose stall; b. Thin-wing stall; c. Mixed type stall; d. Trailing edge stall; e. Stall patterns; f. Nose radius; g. Camber; h. Definition of y_{125}

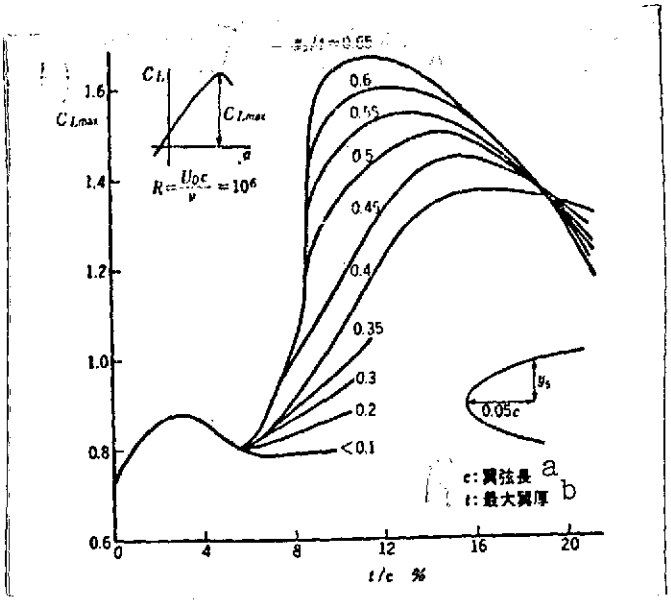

Fig. 5. Variation of C_{Lmax} with nose shape [7].

Key: a. c: wing chord length; b. t: maximum profile thickness.

From the mid-1940's, the objective of research began to shift toward the improvements of high-speed characteristics such as the rapid increase in drag at transonic speeds [5]. However, due to the extreme complexity of the flow around the airfoil section at transonic speeds, it was not possible to determine the shape or pressure distribution which would improve the characteristics, and the systematic development of airfoils gradually fell out of use. With the development of airfoils in this state of temporary standstill, researchers mainly turned to experiments in their efforts to find explanations of the phenomena and methods for improvement. This led to the elucidation of such aspects as the relationships of the profile and thickness of the wing nose to the maximum lift coefficient at the stall characteristics [6, 7] (Figs. 4 and 5). These findings were applied, among other things, to the improvement of the low-speed characteristics of relatively thin airfoils used in high-speed aircraft.

In our country, the late 1930's saw the perfection of practical airfoil theories [8, 9], which were used in the development of various types of airfoils including laminar flow airfoils. After the war, however, practically no substantial development of airfoils was undertaken until the late 1960's. The situation is similar in West Germany too. Research into airfoils went on uninterruptedly in countries such as Great Britain and France, which continued their development of aircraft during and after the war. But since the emphasis of their research was on the improvements of the transonic characteristics to accompany the development of faster aircraft, a systematic development of airfoils was not conducted as in the case of the United States. They adopted the method of constructing new airfoils to meet the requirements of airframes on a trial-and-error basis with the existing airfoils as the starting point.

Since the characteristics of the various NACA airfoil types are known through data from wind tunnel tests, and since the airfoils are available in a wide range of combinations of profile thickness and design lift coefficients, they are being widely used even today.

Meanwhile, a gradual reevaluation of the NACA laminar flow airfoils began to take place from the mid-1950's, and this led to the confirmation of the feasibility of developing airfoils of superior characteristics [10]. In addition, we now have a good prospect that it will soon be possible to estimate airfoil characteristics which take the effects of the boundary layer into consideration [11]. When the use of computers became practical in the 1960's, it became easier to calculate the pressure distribution around the airfoil section. Furthermore, there was an improvement in the accuracy of the calculation of the boundary layer characteristics, so that by now it has become possible to design airfoils which meet the required specifications from the theoretical calculations as far as subsonic airfoils (below velocity of sound at every point on the wing surface) are concerned.

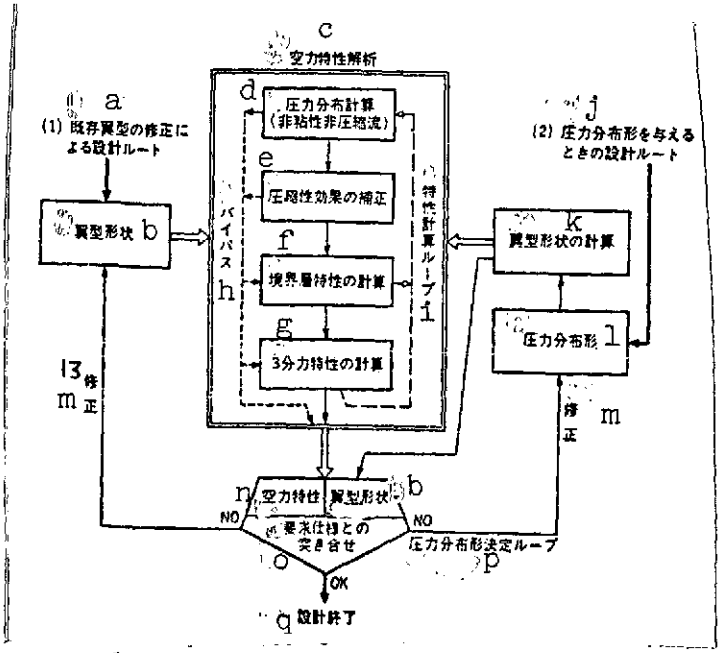

Fig. 6. Design process.

Key: a. (1) Design route using correction of existing airfoils; b. Airfoil profile; c. Analysis of aerodynamic characteristics; d. Calculation of pressure distribution (nonviscous, imcompressible flow); e. Correction for compressibility effect; f. Calculation of boundary layer characteristics; g. Calculation of three-component characteristics; h. Bypass; i. Characteristic calculation loop; j. (2) Design route when giving pressure distribution pattern; k. Calculation of airfoil shape; l. Pressure distribution pattern; m. Correction; n. Aerodynamic characteristics; o. Comparison with required specifications; p. Pressure distribution pattern determination loop; q. Completed design

3. Design Process

There are two routes by which an airfoil which satisfies given specification requirements may be designed (Fig. 6).

1. correction of existing airfoils

The analysis of characteristics and the correction of profiles are repeated.

2. airfoil profiles sought by obtaining pressure distribution pattern.

First, the airfoil calculations and the pressure distribution patterns are corrected repeatedly until a pressure distribution pattern which satisfies the required specifications concerning the airfoil profile is obtained. Next, the characteristics are analyzed and compared with the required aerodynamic specifications and, if necessary, the airfoil section or the pressure distribution pattern is corrected.

Although it is possible to complete the design by route 1 alone, this would be unsuitable when the differences between the initially given airfoil characteristics and the required specifications to be satisfied are large, since the number of repetitions would be increased. In such a case, it would be better first of all to grasp the relationship between the aerodynamic characteristics and the pressure distribution pattern by means of theoretical calculations or the analysis of wind tunnel test results, then to determine the airfoil profile by means of calculations through the entirety of route 2, and finally to embark on the actual designing through route 1. Furthermore, route 2 is indispensable for the designing of airfoils with special pressure distributions. /4

4. Establishment of Required Specifications

The airfoil section must satisfy not only requirements in terms of aerodynamic characteristics, but also requirements in terms of the geometric profile.

First of all, the principal requirements in terms of aerodynamic characteristics (Fig. 7A) are as follows:

(1) Maximum Lift Coefficient C_{Lmax}

This should be as high as possible. It is necessary to make the curvature of the leading edge large to prevent separation at the nose, while the pressure climb at the back of the wing should be slight in order to delay separation at the trailing edge.

(2) Minimum Drag Coefficient C_{D0}

This should be as low as possible. To this end, it is necessary to design the airfoil in such a way that the boundary

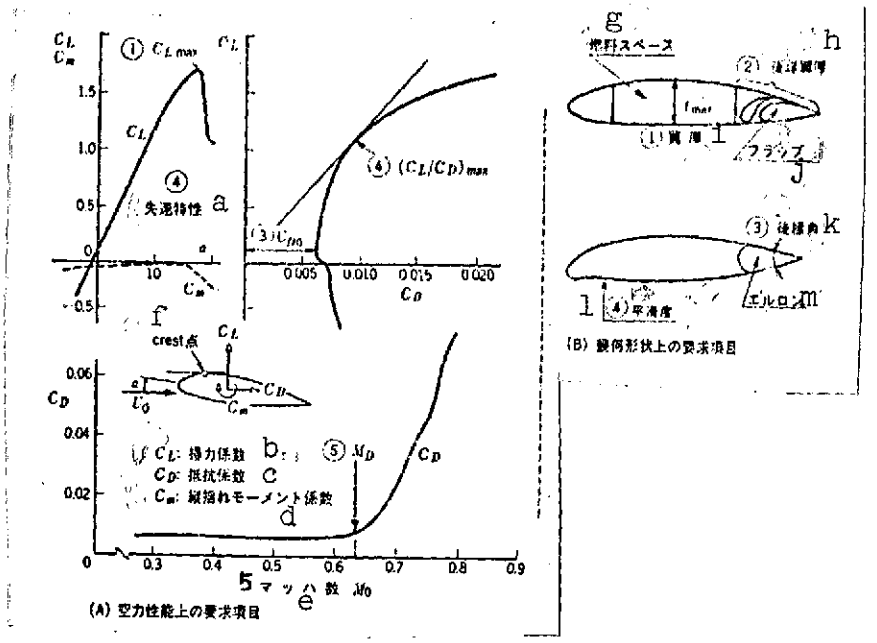

Fig. 7. Principal requirements in airfoil design.
A. Requirements in aerodynamic performance.
B. Requirements in terms of geometric profile

Key:
a. Stall characteristics
b. C_L: lift coefficient
c. C_D: drag coefficient
d. C_m: pitching moment coefficient
e. Mach number
f. Crest point
g. Fuel space
h. Trailing edge profile thickness
i. Profile thickness
j. Flap
k. Trailing edge angle
l. Smoothness
m. Aileron

layer is maintained as a laminar flow as far as the rear of the wing, and, at the same time, separation does not occur at the trailing edge.

(3) Maximum Lift-Drag Ratio $(C_L/C_D)_{max}$

This should be as high as possible. The pressure distribution must be such that a high lift is obtained while separation of the boundary layer is suppressed.

(4) Stall Characteristics

It is required that a rapid decrease in lift or changes in the pitching moment do not occur. It is therefore necessary to design a pressure distribution pattern in which the spread of separation with respect to the angle of incidence is mild, as well as to make the curvature of the nose large.

(5) Mach Number of Rapid Drag Increase M_D

This should be as high as possible. One solution is to maintain the speed at the crest point (Fig. 7A) below the local velocity of sound.

Next, there are the following requirements concerning the geometric profile (Fig. 7B).

(1) Maximum Profile Thickness t_{max}

This should be as thick as possible from the standpoint of fuel space and structural strength.

(2) Profile Thickness Distribution of Trailing Edge

Ample space for housing the high lift device (flap) and the leg is necessary. Also, an extremely thin trailing edge is not practical from the standpoint of structural strength.

(3) Trailing Edge Angle

This must not be greater than a certain angle or the effectiveness of the aileron may be impaired.

(4) Smoothness

Sudden changes in the curvature or surface depressions must be avoided as much as possible.

What is evident here is that it is not always possible to design an airfoil which would satisfy arbitrarily given specifications, because some of these requirements are in conflict with each other. Consequently, it is first of all necessary to carry out adjustments in the required specifications on the basis of the available data (for instance, Figs. 4 and 5) before entering the design phase. Secondly, it is also necessary to make appropriate corrections in the course of the design process, so that needless efforts may be avoided.

5. Analysis Method for Aerodynamic Characteristics

The most reliable method of analyzing the characteristics of an airfoil is the wind tunnel test. But, since this method is both time-consuming and costly, it is not suitable for conducting far-reaching examinations in the initial stage of airfoil design, although it is effective for verifying the characteristics or studying the effects of minor corrections.

The method through calculation still remains ineffectual with respect to conditions in which the effects of separation or compressibility are major, but it has advanced to the point of providing sufficient accuracy for the analysis of characteristics in the vicinity of the design point (in the range of normally used Mach numbers and lift coefficients).

The analysis of characteristics for a given airfoil section profile may be divided into the following four steps (Fig. 6):

1. calculation of pressure distribution (nonviscous, incompressible flow);

2. correction for compressible flow;

3. calculation of boundary layer characteristics;

4. calculation of three-component characteristics.

It is not always necessary to go through all these steps. In the initial stage of the design process, steps 2 or 3 are sometimes bypassed.

5.1. Calculation of Pressure Distribution

Many methods have been developed, but it would seem that on the basis of suitability for numerical value calculations and applicability to both the pressure distribution calculation and the airfoil profile calculation, Weber's method [12] is suitable for wings with a small camber, and Oeller's method [13], which was developed as a theory in the calculation of cascade blades, is suitable for wings with a large camber.

5.1.1. Weber's Method

Although this method can only be applied to airfoil sections of relatively thin camber or profile thickness, since it is based on the microdisturbance theory, its accuracy has been confirmed to be sufficient in practical use within the possible range of its application. By now, its application has been expanded even to analysis of airfoil characteristics which take into consideration compressibility and boundary layer effects, and good agreement has been obtained with experimental values. Another advantage of this method is that it is applicable to the design and characteristics analysis of three-dimensional wings. It is currently being applied widely in this area.

In this method, it is assumed that the wing surface is represented by a combination of the camber and thickness. It is noted that the airfoil coordinates are dimensionless along the wing chord.

$$\begin{aligned} &\text{camber} && y_c = 0.5\ (y_{UPPER} + y_{LOWER}) \\ &\text{profile thickness} && y_t = 0.5\ (y_{UPPER} - y_{LOWER}) \end{aligned} \qquad (1)$$

Assuming that the flow around the airfoil can be expressed in terms of the vortex $\gamma(x)$ and effusion $q(x)$ distributed on the line of the wing chord, their intensities are determined by the boundary condition

$$\frac{dy}{dx} = \frac{v}{U_0 + u} \fallingdotseq \frac{v}{U_0} \qquad (2)$$

where U_0: velocity of uniform flow

u, v: disturbance velocities in the direction of the x and y axes.

This boundary condition can be further divided into the two conditions of

$$\left.\begin{aligned} &\frac{dy_c}{dx} = \frac{v_c}{U_0} \\ &\gamma(1) = 0 \quad \text{(Kutta's condition at trailing edge)} \end{aligned}\right\} \qquad (3) \quad /5$$

$$\frac{dy_t}{dx} = \frac{v_q}{U_0} \qquad (4)$$

The case of angle of incidence $\alpha = 0$ is first considered.

The velocity $u_\gamma(x)$, which is induced by vortex distribution γ in the direction of the x axis, is given by equation (5), which solves equation (3).

$$\left(\frac{u_r}{U_0}\right)_{\alpha=0} = \pm\frac{\Gamma}{2U_0} = \pm\frac{1}{\pi}\sqrt{\frac{1-x}{x}} \cdot \int_0^1 \frac{dy_c}{d\xi}\sqrt{\frac{\xi}{1-\xi}}\cdot\frac{d\xi}{x-\xi} \tag{5}$$

+: upper surface; −: lower surface

Similarly, the induced velocity $u_q(x)$ is given by equation (6), which solves equation (4).

$$\left(\frac{u_q}{U_0}\right)_{\alpha=0} = 1+\frac{1}{\pi}\int_0^1 \frac{dy_t}{d\xi}\frac{d\xi}{x-\xi} \tag{6}$$

Next, the velocity increase without the angle of incidence is given by equation (7), which adds the effect of profile thickness to the value in the case of a flat panel.

$$\left(\frac{u_r}{U_0}\right)_{\alpha=0} = \pm\sin\alpha\sqrt{\frac{1-x}{x}}\int_0^1\left\{\frac{dy_t}{d\xi}-\frac{y_t}{2\xi(1-\xi)}\right\}\frac{d\xi}{x-\xi} \tag{7}$$

When the uniform flow rate U_0 and the induced velocities above are combined, the velocity distributions on the upper and lower surfaces of the wing are obtained. Normally, equation (8), which contains a correction for improving the accuracy in the vicinity of the nose, is used.

$$\frac{U(x)}{U_0} = \frac{1+S^{(1)}(x)\pm S^{(4)}(x)\pm\sin\alpha\sqrt{\frac{1-x}{x}}\{1+S^{(3)}(x)\}}{\sqrt{1+\{S^{(2)}(x)\pm S^{(5)}(x)\}^2}} \tag{8}$$

where

$$\begin{aligned}
S^{(1)}(x) &= \frac{1}{\pi}\int_0^1 \frac{dy_t}{d\xi}\frac{d\xi}{x-\xi}\\
S^{(2)}(x) &= \frac{dy_t}{dx}\\
S^{(3)}(x) &= \frac{1}{\pi}\int_0^1\left\{\frac{dy_t}{d\xi}-\frac{y_t}{2\xi(1-\xi)}\right\}\frac{d\xi}{x-\xi}\\
S^{(4)}(x) &= \frac{1}{\pi}\sqrt{\frac{1-x}{x}}\int_0^1 \frac{dy_c}{d\xi}\sqrt{\frac{\xi}{1-\xi}}\frac{d\xi}{x-\xi}\\
S^{(5)}(x) &= \frac{dy_c}{dx}
\end{aligned} \tag{9}$$

During the actual calculation of numerical values, profile thickness $y_t(x_\nu)$ and camber $y_c(x_\nu)$ are sought with respect to the (N - 1) number of the x coordinates

$$x_\nu = 0.5\left(1+\cos\frac{\nu\pi}{N}\right) \quad \nu = 1, \cdots\cdots, N-1 \tag{10}$$

before $S^{(1)}(x_\nu),\ldots,S^{(5)}(x_\nu)$ are calculated from equations (11).

$$\left.\begin{aligned}
S^{(1)}(x_\nu) &= \sum_{\mu=1}^{N-1} SC1(\mu,\nu)\, y_t(x_\nu) \\
S^{(2)}(x_\nu) &= \sum_{\mu=1}^{N-1} SC2(\mu,\nu)\, y_t(x_\nu) \\
S^{(3)}(x_\nu) &= \sum_{\mu=1}^{N-1} SC3(\mu,\nu)\, y_t(x_\nu) + SC3(N,\nu)\sqrt{\frac{\rho}{2c}} \\
S^{(4)}(x_\nu) &= \sum_{\mu=1}^{N-1} SC4(\mu,\nu)\, y_c(x_\nu) \\
S^{(5)}(x_\nu) &= \sum_{\mu=1}^{N-1} SC5(\mu,\nu)\, y_c(x_\nu)
\end{aligned}\right\} \tag{11}$$

In the above, ρ is the nose radius and c is the wing chord length. The coefficients $SC_1(\mu,\nu)\ldots SC_5(\mu,\nu)$ are given in the Appendix.

The advantage of Weber's method is that the above coefficients are defineduuniquely by giving the partition number N, regardless of the airfoil type, so that the velocity distribution can be calculated easily for any given airfoil section. As already stated, the accuracy of this method, which is based on the microdisturbance theory, deteriorates for large camber, profile thickness and angle of incidence (Fig. 8), but its practicality is sufficient with respect to the vicinity of the design point of airfoils in the range of common use in aircraft (Fig. 9). With respect to cascade blades, there is Schlichting's method, which resembles Weber's method, but we will omit it on this occasion.

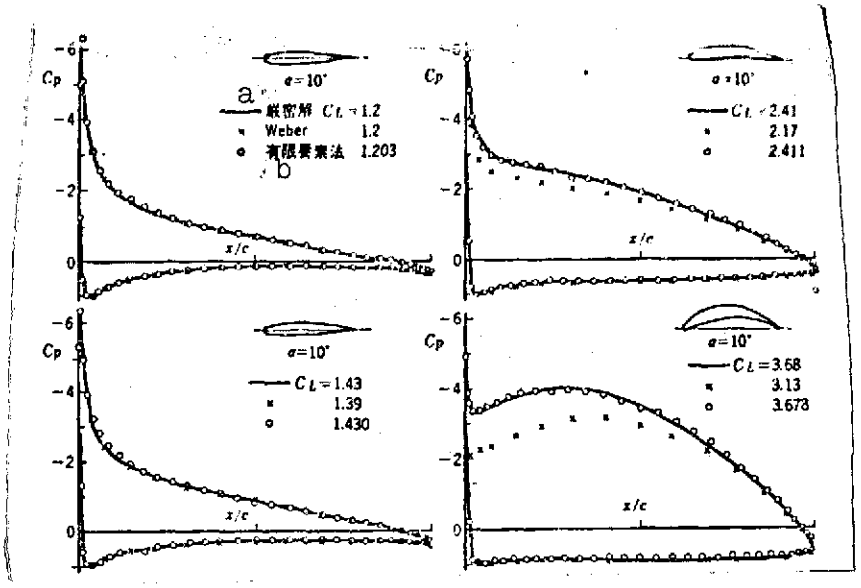

Fig. 8. Accuracy check on Weber's method and finite element method [15].

Key: a. Strict solution
b. Finite element method

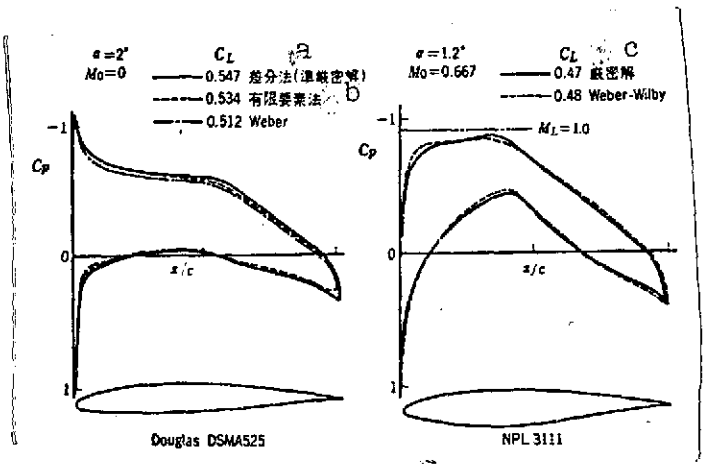

Fig. 9. Comparison of Weber's method with other more exact methods [17, 18].

Key: a. Difference calculus (semi-strict solution); b. Finite element method; c. Strict solution

5.1.2. Oeller's Method (Finite Element Method)

In this method, the vortex is distributed over the wing surface, but, unlike Weber's method, there is no restriction on its application.

The flow function of the flow around the wing can be expressed as

$$+\frac{1}{2\pi}\oint \gamma(s')K(s, s')ds \tag{12}$$

But it has to be $\psi = \psi_0 = \text{const}$ along the wing surface, since there

is only one line of flow on the wing surface. When the vortex distribution $\gamma(s)$ is defined to satisfy this condition, the velocity on the wing surface U(s) is given simply by

$$U(s)=\gamma(s) \tag{13}$$ /6

The function K(s,s') is

$$K(s, s')=-\ln r=-\ln\sqrt{(x-\xi)^2+(y-\eta)^2} \tag{14}$$

for a single airfoil, and

$$K(s, s')=-\ln R=-\ln\sqrt{2\left\{\cosh\frac{2\pi(x-\xi)}{t}-\cos\frac{2\pi(y-\eta)}{t}\right\}} \tag{15}$$

for cascade blades (Fig. 10).

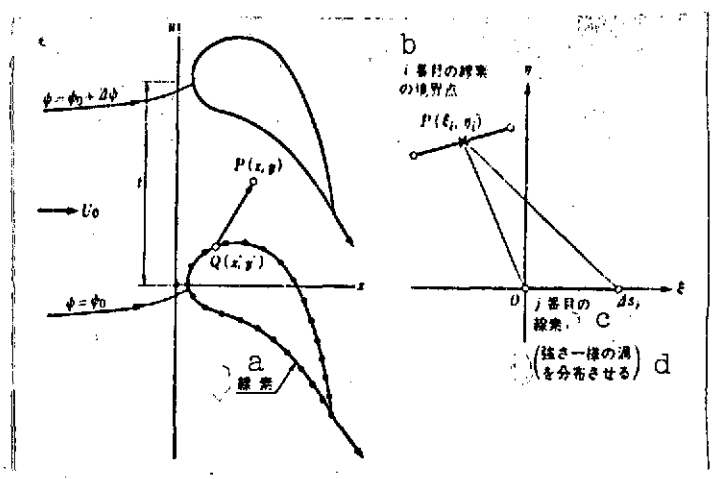

Fig. 10. Calculation model for Oeller's method.

Key: a. Line element; b. Boundary point of i-th line element; c. j-th line element; d. (Vortex of uniform density is distributed.)

Let us discuss the calculation procedure for a single airfoil. The wing surface is first divided into N number of small elements. Assuming that the vortex distribution is uniform on these elements, the integral is replaced with a finite sum, and it is further assumed that the boundary condition mentioned earlier is satisfied at the midpoint of each element. In this manner, N number of simultaneous linear equations are obtained with respect to N + 1 number of unknown

quantities (intensity γ_i of N number of vortices and flow function value ψ_0). By solving N + 1 number of simultaneous equations

$$\left.\begin{aligned} &\frac{1}{2\pi}\sum_{j=1}^{n} K_{ij}\gamma_j+\psi_0=y_i U_0\cos\alpha-x_i U_0\sin\alpha \\ &\qquad\qquad\qquad\qquad\qquad\qquad i=1,\ \cdots\cdots,\ N \\ &\gamma_1=-\gamma_N \end{aligned}\right\} \tag{16}$$

which consist of the above combined Kutta's condition at the trailing edge, the vortextintensity, which is to say the velocity, is obtained.

K_{ij} is the influence coefficient from the j-th element to the i-th boundary point. By setting the system of coordinates as shown in Fig. 10, it can be calculated by the following equations.

$$\left.\begin{aligned} K_{ij}=&\frac{1}{2}[(\Delta s_j-\xi_i)\ln\{(\Delta s_j-\xi_i)^2+\eta_i^2\} \\ &+\xi_i\ln(\xi_i^2+\eta_i^2)]-\Delta s_j \\ &+\eta_i\left\{\tan^{-1}\left(\frac{\eta_i}{\Delta s_j-\xi_i}\right)-\tan^{-1}\left(\frac{\eta_i}{-\xi_i}\right)\right\} \\ &\qquad\qquad\qquad\qquad : i\neq j \\ =&\Delta s_j\left\{\ln\left(\frac{\Delta s_j}{2}\right)-1\right\} \quad : i=j \end{aligned}\right\} \tag{17}$$

In the case of cascade blades, it is necessary to further subdivide the j-th element and obtain it by numerical integration. However, the above equation may be used in the case of i = j.

The calculation accuracy of Oeller's method is of the same degree as that of other finite element calculation methods [14, 15]. A comparison with the strict solution is shown in Fig. 8. The accuracy is extremely good.

5.2. Correction for Compressibility Effect

When the velocity of uniform flow becomes high, it is no longer possible to ignore the effect of compressibility. The

following methods, which are correction methods based on the approximation theory, whose practicality has been confirmed through comparison with experimental results, can be applied.

5.2.1. Karman-Tsien Method

This is often used because of its simplicity. First of all, the velocity distribution U_i is calculated for an incompressible flow, so that the pressure coefficient C_{pi} is obtained.

$$C_{pi}=1-\left(\frac{U_i}{U_0}\right)^2 \tag{18}$$

It is assumed that the pressure coefficient C_p corrected for the compressibility effect is given by the following equation

$$C_p=\frac{C_{pi}}{\sqrt{1-M_0^2}+\dfrac{M_0^2 C_{pi}}{2(1+\sqrt{1-M_0^2})}} \tag{19}$$

5.2.2. Wilby's Method [16]

This method is suitable for application to the calculation of pressure distribution by means of Weber's method.

$$\left.\begin{aligned}\frac{U}{U_0}&=\frac{1+\dfrac{S^{(1)}+S^{(4)}}{B}\pm\dfrac{\sin\alpha}{B}\sqrt{1-\dfrac{x}{c}}\left(1+\dfrac{1}{B}S^{(3)}\right)-\dfrac{1}{2}\left(\dfrac{\sin\alpha}{B}\right)^2}{\sqrt{1+\left(\dfrac{S^{(2)}\pm S^{(5)}}{B}\right)^2}}\\ B&=\sqrt{1-M_0^2(1-M_0^2C_{pi})}\end{aligned}\right\} \tag{20}$$

The pressure coefficient is calculated using the following equation.

$$C_p=\frac{1}{0.7M_0^2}\left[\left\{1+0.2M_0^2\left(1-\frac{U^2}{U_0^2}\right)\right\}^{3.5}-1\right] \tag{21}$$

Since the accuracy of correction varies according to the airfoil shape as shown in Fig. 11, it is not possible to state unconditionally which method is superior.

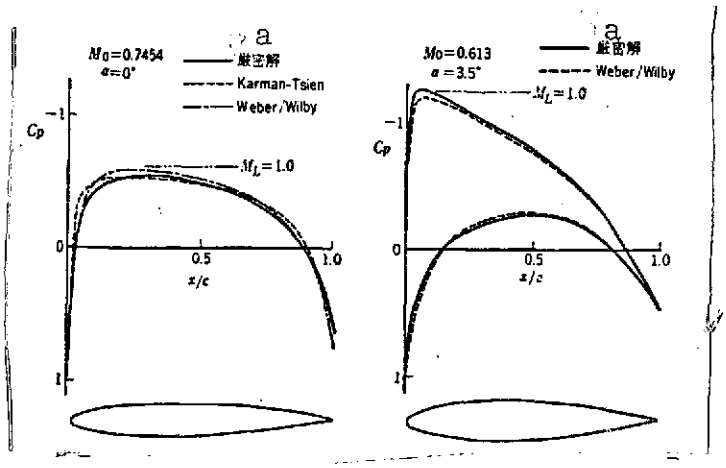

Fig. 11. Accuracy check on compressibility correction methods [17, 18]. Wilby's method.

Key: a. Strict solution.

5.2.3. Stockman's Method [19]

This is a method which was discovered experimentally as a correction method for internal flows, such as cascade blades or jet engine intake. In order to apply this method, the velocity distribution U_i on the wing surface and the mean flow velocity $\overline{U}_i$ between the cascade blades are calculated first under the assumption that the flow is incompressible. Next, mean density $\overline{\rho}_c$ is sought under the assumption that the flow between the cascade blades is a compressible, one-dimensional flow, and then the velocity U_c on the wing surface is calculated using the following equation.

$$U_c = U_i \left(\frac{\rho_i}{\overline{\rho}_c} \right)^{U_i/\overline{U}_i} \tag{22}$$

Fig. 12 shows an example of the application of this method to the pressure distribution on the interior of an air intake.

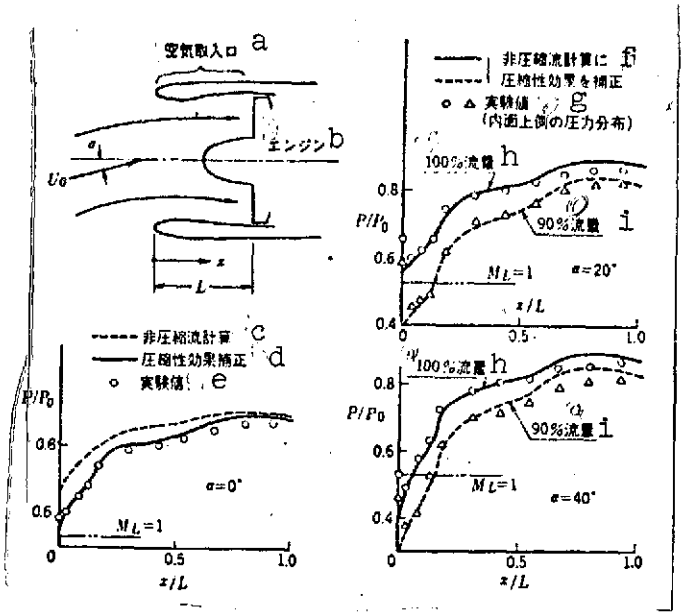

Fig. 12. Accuracy check on compressibility correction method [17]. Stockman's method.

Key: a. Air intake; b. Engine; c. Incompressible flow calculation; d. Correction for compressibility effect; e. Experimental value; f. Incompressible flow calculation corrected for compressibility effect; g. Experimental values (pressure distribution on upper side of inner surface); h. 100% flow volume; i. 90% flow volume

5.3. Calculation of Boundary Layer Characteristics

Most of the aerodynamic characteristics of airfoils or cascade blades are determined by the behavior of the boundary layer on the wing surface. In other words, the maximum lift or the stall characteristics are determined by the manner in which separation of the boundary layer occurs, while the minimum drag is determined by the position of transition of the boundary layer, as well as by the manner in which the boundary layer develops thereafter.

Due to recent advances in the area of calculation methods for the turbulent flow boundary layer, the accuracy of the estimation of the drag in the vicinity of the design point has been improved considerably. However, while the accuracy of estimation of the separation point when the velocity distribution after the occurrence of separation has been given has become quite high, a method has not yet been established for the estimation of the velocity distribution when it is accompanied by separation. It is therefore impossible at present to seek the maximum lift or stall characteristics quantitatively. Nevertheless, it is still possible to estimate whether separation occurs or not, so that such estimation methods can be effective in

/7

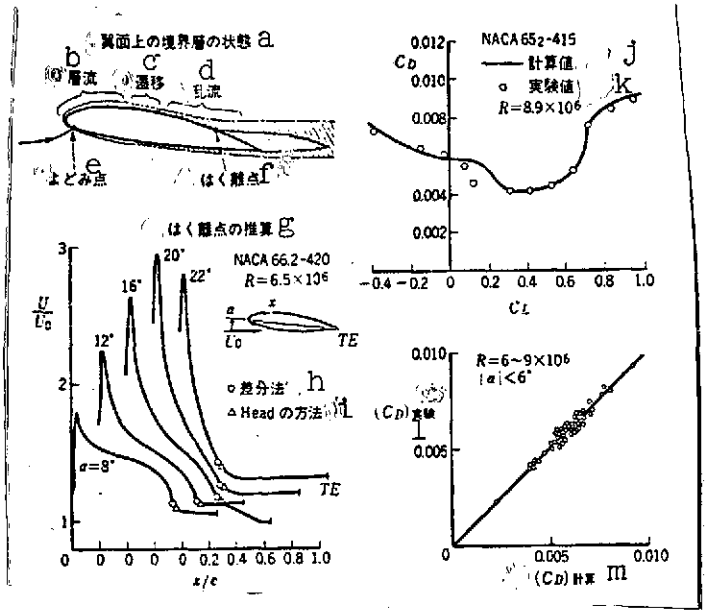

Fig. 13. Estimation of separation point of boundary layer and drag coefficient [23, 24].

Key: a. Boundary layer condition on wing surface; b. Laminar flow; c. Transition; d. Turbulent flow; e. Stagnation point; f. Separation point; g. Estimation of separation point; h. Difference calculus; i. Head's method; j. Calculated value; k. Experimental values; l. Experiment (C_D); m. Calculated (C_D)

qualitative studies or the improvement of the characteristics.

As shown in Fig. 13, the boundary layer is a laminar flow at the airfoil nose, and undergoes a transition to turbulent flow at a certain point. When the decrease in the velocity on the wing surface, that is, the increase in pressure, is rapid, separation can occur either in the laminar flow portion or in the turbulent flow portion.

On this occasion, we will show one method for calculating the boundary layer characteristics in an incompressible flow. In practice, we use a calculation method in which these characteristics are corrected for the compressibility effect [22], but it will be omitted in this report.

5.3.1. Laminar Flow Boundary Layer

By means of the Thwaite method [20], the momentum thickness θ may be obtained by the following integration process, provided that the velocity distribution U can be obtained.

$$\left(\frac{\theta}{c}\right)^2=\frac{0.45}{R\left(\frac{U}{U_0}\right)^6}\int_0^{x/c}\left(\frac{U}{U_0}\right)^5 d\left(\frac{x}{c}\right) \tag{23}$$

Here R is the Reynolds number which is defined by the following equation in terms of the uniform flow velocity U_0, chord length c, and the kinetic viscosity coefficient ν of the fluid.

$$R=\frac{U_0 c}{\nu} \tag{24}$$

In addition, θ is a quantity which is defined in the following manner from the velocity distribution u inside the boundary layer.

$$\theta=\int_0^\infty \frac{u}{U}\left(1-\frac{u}{U}\right)dy \tag{25}$$

In this method, it is assumed that separation occurs at the point where the following equation is satisfied.

$$\left(\frac{\theta}{c}\right)^2=-\frac{0.090}{R}\left\{\frac{d\left(\frac{U}{U_0}\right)}{d\left(\frac{x}{c}\right)}\right\}^{-1} \tag{26}$$

5.3.2. Transition

Let the point at which the following experimental equation of Michel [23] is satisfied be the transition point.

where

$$\left.\begin{aligned} &R_\theta=1.174\left(1+\frac{22\,400}{R_x}\right)R_x^{0.46} \\ &0.1\times10^6\leqq R_x\leqq 60\times10^6 \\ &R_\theta=\frac{U\theta}{\nu},\quad R_x=\frac{Ux}{\nu} \end{aligned}\right\} \tag{27}$$

Although there is a certain distance between the starting point and the end point of transition, we will carry out the

calculation of the turbulent flow boundary layer on the assumption that the transition occurs at the single point obtained from equation (27) for the sake of convenience of calculation. Also, when the laminar flow boundary layer undergoes re-adhesion after separation, the separation point will be considered as the transition point.

5.3.3. Turbulent Flow Boundary Layer

Head's method [21] is not only easy to use, but also is in good agreement with the experimental values. In this method, the momentum thickness θ is obtained by solving the following differential equation.

$$\frac{d\theta}{dx}+(H+2)\frac{\theta}{U}\frac{dU}{dx}=\frac{C_f}{2} \tag{28}$$

C_f is the friction coefficient for which the following equation is widely used.

$$C_f=0.246(10)^{-0.678H}(R_\theta)^{-0.268} \tag{29}$$

Here, H is the form coefficient and is a ratio between θ and displacement thickness δ*.

$$\left.\begin{aligned} H&=\frac{\delta^*}{\theta}\\ \delta^*&=\int_0^\infty\left(1-\frac{u}{U}\right)dy \end{aligned}\right\} \tag{30}$$

In order to solve equation (30), it is necessary to know the value of H. This is obtained by the following equations.

$$\frac{1}{U}\frac{d(U\theta H_1)}{dx}=0.0299(H_1-3.0)^{-0.6169} \tag{31}$$

$$H_1 \equiv G(H) = \begin{cases} 0.8234(H-1.1)^{-1.287} & H \leqq 1.6 \\ 1.5501(H-0.6778)^{-3.064}+3.3 & H \geqq 1.6 \end{cases} \quad (32)$$

It is noted that the initial values of θ and H, θ_0 and H_0, are necessary for the above calculations. These are obtained from the θ_T and H_T at the transition point, which was obtained in the calculation of the laminar flow boundary layer in the following manner.

$$\theta_0 = \begin{cases} \theta_T & R_{\theta T} \geqq 320 \\ \dfrac{320\nu}{U_T} & R_{\theta T} < 320 \end{cases} \quad (33)$$

$$H_0 = H_T - (1.19 + 0.1 \ln R_{\theta T} - 0.005(\ln R_{\theta T})^2) \quad (34)$$

Separation in the turbulent flow boundary layer occurs when the value of H is between 1.8 and 2.4. It may seem that the difference between these upper and lower limits of H is too large. However, since the increase in H in the vicinity of the separation point is rapid, this difference becomes small in terms of the position of the separation point. It is also in good agreement with the results obtained by means of a stricter method (difference calculus) (Fig. 13). /8

5.3.4. Wake

In order to obtain the total drag, which includes the pressure drag and the frictional drag, the momentum thickness θ_∞ on the infinite extension of the wake becomes necessary. For this, the following Squire-Young equation [23] is used.

$$\theta_\infty = \theta_{TE}\left(\frac{U_{TE}}{U_0}\right)^{0.5(H_{TE}+5)} \quad (35)$$

5.4. Calculation of Three-Component Characteristics

The lift coefficient and the pitching moment coefficient are obtained by integrating the pressure distribution on the wing surface.

$$C_L = \int_0^1 (C_{p\,\mathrm{LOWER}} - C_{p\,\mathrm{UPPER}})\, d\left(\frac{x}{c}\right)$$
$$C_m = \int_0^1 (C_{p\,\mathrm{LOWER}} - C_{p\,\mathrm{UPPER}}) \left(\frac{x_0 - x}{c}\right) d\left(\frac{x}{c}\right) \qquad (36)$$

In addition, the drag coefficient can be calculated using equation (37).

$$C_D \fallingdotseq 2((\theta_{TE})_{\mathrm{UPPER}} + (\theta_{TE})_{\mathrm{LOWER}}) \left(\frac{U_{TE}}{U_0}\right)^{0.5(H_{TE}+5)} \qquad (37)$$

As illustrated by Fig. 13, the drag value is in good agreement with experimental values where the angle of incidence is small. But since there is a large difference between experimental and calculated values of the pressure distribution (Fig. 14), the accuracy is not good in the estimation of C_L and C_m. This is due to the practical deformation of the airfoil profile due to the development of the boundary layer. According to Powell [17], the effect of this phenomenon can be considered in terms of the following three components (Fig. 15):

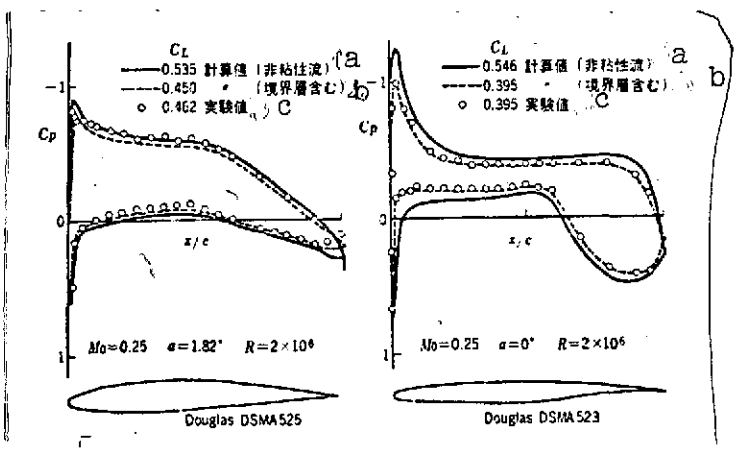

Fig. 14. Boundary layer effect on pressure distribution [18].

Key: a. Calculated value (non-viscous flow); b. Calculated value (including boundary layer); c. Experimental values

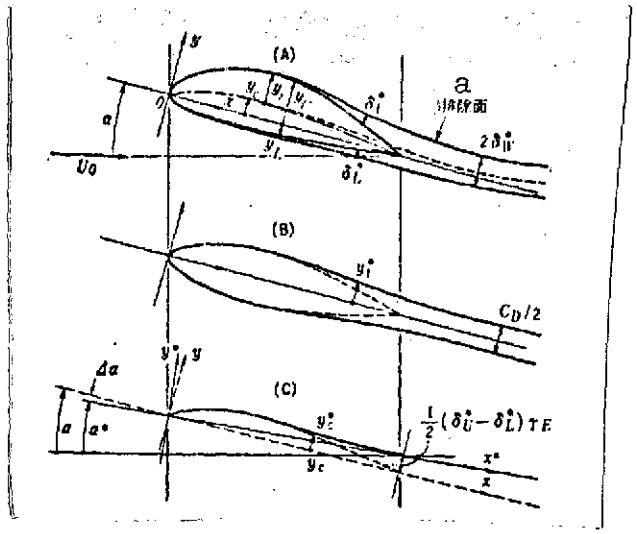

Fig. 15. Calculation model for estimation of boundary layer effect (17, 25]. Powell's method.

A. Flow model concept. The form produced by the displacement surface is considered as an independent airfoil section.
y_U: upper coordinate
y_L: lower coordinate
y_c: camber
y_t: profile thickness
δ_U^*: upper displacement thickness
δ_L^*: lower displacement thickness
δ_W^*: Wake displacement thickness

B. Equivalent profile thickness

$$y_t^* = y_t + \frac{1}{2}(\delta_U^* + \delta_L^*)$$

C. Equivalent camber and change in angle of incidence

$$y_c^* = y_c + \frac{1}{2}(\delta_U^* - \delta_L^*) + x\tan\Delta\alpha$$
$$\alpha^* = \alpha - \Delta\alpha$$
$$\tan\Delta\alpha = \frac{1}{2}(\delta_U^* - \delta_L^*)_{TE}$$

Key: a. Displacement surface

(1) change in profile thickness;

(2) change in camber;

(3) change in angle of incidence.

When Weber's method is used, equation (9) is corrected to enable the calculation of $S^{(1)}$, $S^{(2)}$ and $S^{(3)}$ for profile thickness distribution y_t^*, which includes the wake, and then the velocity distribution is sought from $S^{(4)}$ and $S^{(5)}$, obtained from the corrected camber y_c^*, as well as the corrected angle of incidence α^* [25]. When Oeller's method is used, the velocity distribution is sought with respect to a form which is obtained by cutting off the wake of an equivalent airfoil profile at a finite length. After that, the equivalent airfoil profile is readjusted by going through steps 5.2 and 5.3. It is necessary to repeat this process until the pressure distribution pattern is settled. Normally, convergence occurs

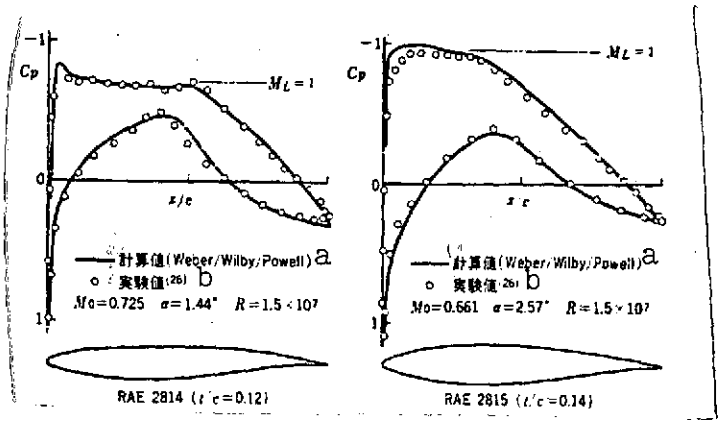

Fig. 16. Example of pressure distribution calculation with corrected boundary layer effect.

Key: a. Calculated value; b. Experimental value

after three or four times. Fig. 16 shows calculation examples using Weber's method.

As already stated, a method which can be applied to cases accompanied by separation has not yet been developed. However, attempts have been made to estimate such characteristics, which are situated outside the design point, by adding a separation domain of an appropriate form onto the equivalent airfoil profile, and there is a good prospect for putting this method to practical use [27].

6. Design Calculation of Airfoil Profile

The case of incompressible flow is considered for the sake of simplicity. When velocity or pressure distribution in a compressible flow is given, it is converted into a velocity distribution for an incompressible flow under an appropriate hypothesis.

6.1. Design Using Weber's Method

Equation (8) is rewritten so that profile thickness y_t and camber y_c become the unknown quantities.

$$\left.\begin{aligned}&\sum_{\mu=1}^{N-1}\{SC1(\mu,\nu)y_t(x_\mu)\pm SC6(\mu,\nu)y_c(x_\mu)\}\\&\quad=\frac{U_\pm(x_\nu)}{U_0}\sqrt{1+(S^{(2)}(x_\nu)\pm S^{(5)}(x_\nu))^2}-1+\frac{1}{2}\sin^2\alpha\\&\qquad-\sin\alpha\sqrt{\frac{1-x_\nu}{x_\nu}}\equiv F_\pm(x_\nu)\\&\nu=1,\cdots\cdots,N-1\end{aligned}\right\}\qquad(38)$$

/9

where

$$+\sin\alpha\sqrt{\frac{1-x_\nu}{x_\nu}}SC3(\mu,\nu)\Bigg| \tag{39}$$

It is indicated that + represents the value on the upper surface and - the value on the lower surface. From equation (38), the following equations are derived.

$$\left.\begin{aligned}&\sum_{\mu=1}^{N-1}SC1(\mu,\nu)y_t(x_\mu)\\&\quad=0.5\{F_+(x_\nu)+F_-(x_\nu)\}\\&\sum_{\mu=1}^{N-1}SC6(\mu,\nu)y_c(x_\mu)\\&\quad=0.5\{F_+(x_\nu)-F_-(x_\nu)\}\end{aligned}\right] \tag{40}$$

Since the right side of these equations are nonlinear functions of y_t and y_c, repeated calculations are required for solving them, but, normally, convergence is obtained after three to five times.

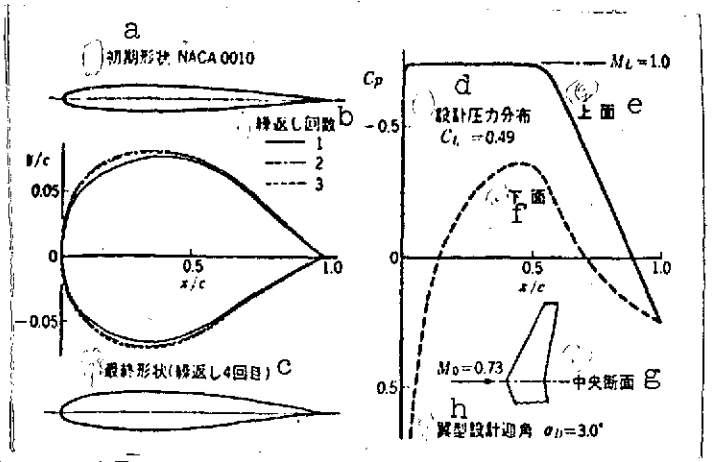

Fig. 17. Example of airfoil profile calculation using Weber's method (center section of a three-dimensional wing).

Key: a. Initial profile; b. Number of repetitions; c. Final profile (fourth repetition); d. Design pressure distribution; e. Upper surface; f. Lower surface; g. Center section; h. Airfoil design angle of incidence

It is noted that it is also possible to introduce the compressibility effect directly into the calculation by using equation (20). A calculation example is shown in Fig. 17.

6.2. Design Using Oeller's Method

The great advantage of this system in design

calculation is that x(s) and y(s) are manifested positively outside the integral, as illustrated by equation (12).

First of all, an appropriate airfoil section is given as the 0-th approximation of the repeated calculation process, and K_{ij} is calculated. ψ_0 is then obtained by solving equation (16). Then a new y(s) is calculated from the given design velocity distribution by means of equation (41). For the convenience of calculation, it is assumed that x(s) does not change.

$$y(s_i)=\frac{1}{U_0\cos\alpha}\left\{x(x_i)U_0\sin\alpha+\psi_0+\sum_{j=1}^{N}K_{ij}U(s_i)\right\} \tag{41}$$

After K_{ij} is obtained and ψ_0 is recalculated for the newly obtained airfoil profile, the velocity $U(s_j)$ at the boundary point is obtained from the calculation of distance s, which is measured along the surface of this airfoil profile. Then, the next approximated value is sought using the above equation. This process is repeated until the profile converges.

It is noted that when the velocities of the upper and lower surfaces are given arbitrarily, it sometimes results in the non-closure of the trailing edge or the intersection of the upper and lower surfaces. It is thus necessary to make appropriate corrections in the velocity distributions in the course of the repetition process [28]. When the velocity distribution and profile thickness distribution of either the upper or lower surface are given, such corrections become unnecessary. Calculation examples are shown in Fig. 18.

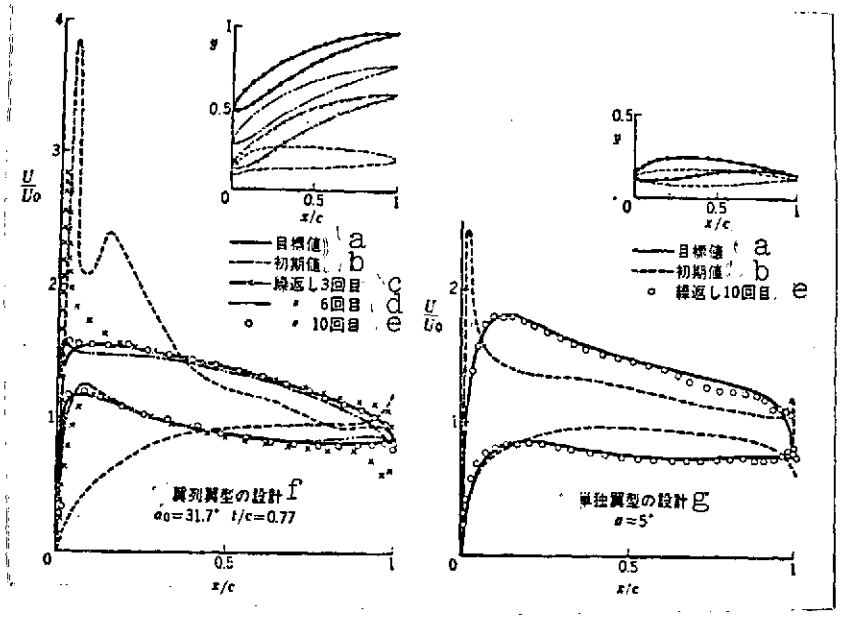

Fig. 18. Examples of airfoil and cascade profiles calculated by the finite element method [28].

Key:
a. Target value
b. Initial value
c. Third repetition
d. Sixth repetition
e. Tenth repetition
f. Cascade section design
g. Single airfoil design

7. Design Examples

Since the analysis of aerodynamic characteristics and airfoil design calculations have become easier, as we have seen, attempts are being made to develop airfoils of better performance than the existing airfoils, as well as airfoils designed for special uses. In this report, we will introduce three examples.

7.1. High Lift, Low Drag Airfoils

By seeking a pressure distribution which would maximize the lift which can possibly be exhibited by the upper wing surface under the condition that the separation of the boundary layer must

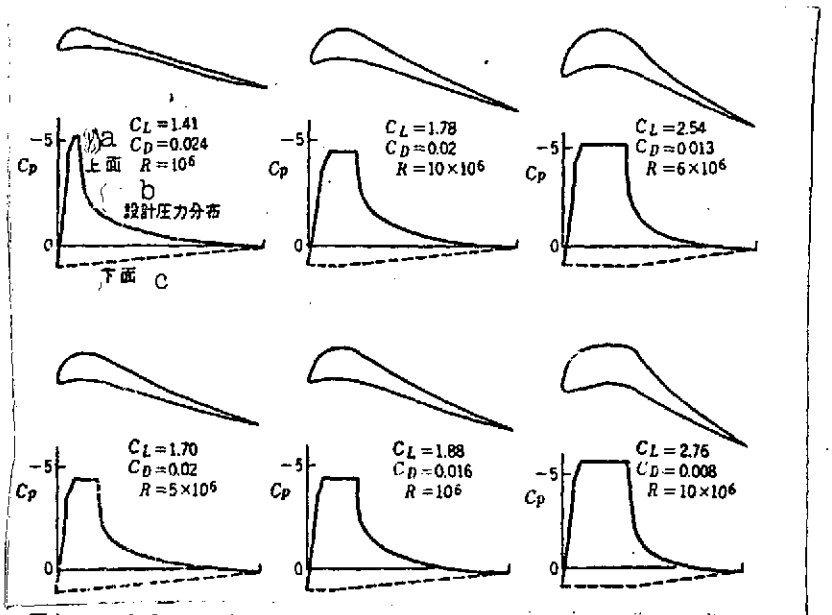

Fig. 19. Some of Liebeck's airfoils [13].

Key: a. Upper surface; b. Design pressure distribution; c. Lower surface

not occur, and then constructing an airfoil which fulfills such criteria, one can obtain a wing of high lift and low drag. A series of airfoils, called Liebeck's airfoils [13], were designed using such a concept. The design lift coefficient is as much as 2.7 in some of these airfoils (Fig. 19). Fig. 20 shows the results of a wind tunnel test conducted on an airfoil whose

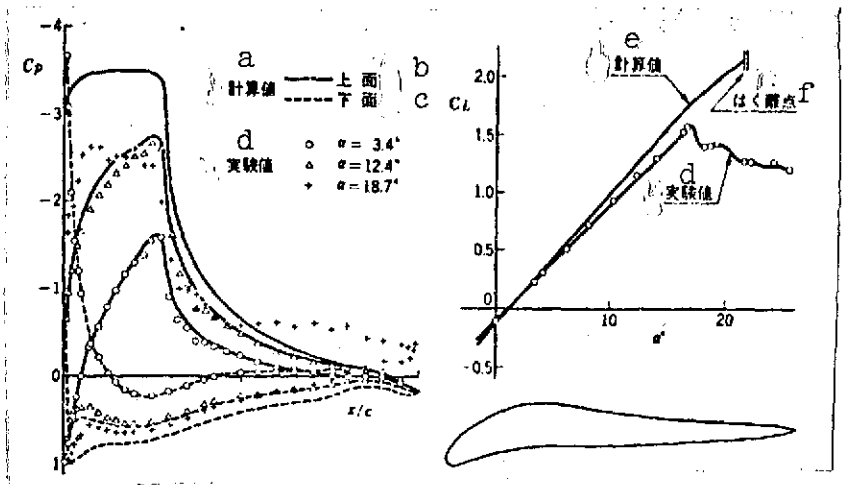

Fig. 20. Experimental results of a Liebeck's airfoil [29].

Key: a. Calculated values
b. Upper surface
c. Lower surface
d. Experimental values
e. Calculated value
f. Separation point

$C_{L\ DESIGN}$ is 2.1. Although the target values are not achieved with this example, it is reported that design characteristics were satisfied in other unpublished results of wind tunnel tests. /10

Nonweiler's low-drag airfoils [30] (Fig. 21) are not necessarily designed for high lift, but some of them have high design lift coefficients. Fig. 22 shows the results of a wind tunnel test for an airfoil whose $C_{L\ DESIGN}$ is 1.39, and the upper limit of whose low drag domain is C_L = 1.89. It is clear that its high lift characteristics have been greatly improved when it is compared to NACA airfoils of similar profile thicknesses.

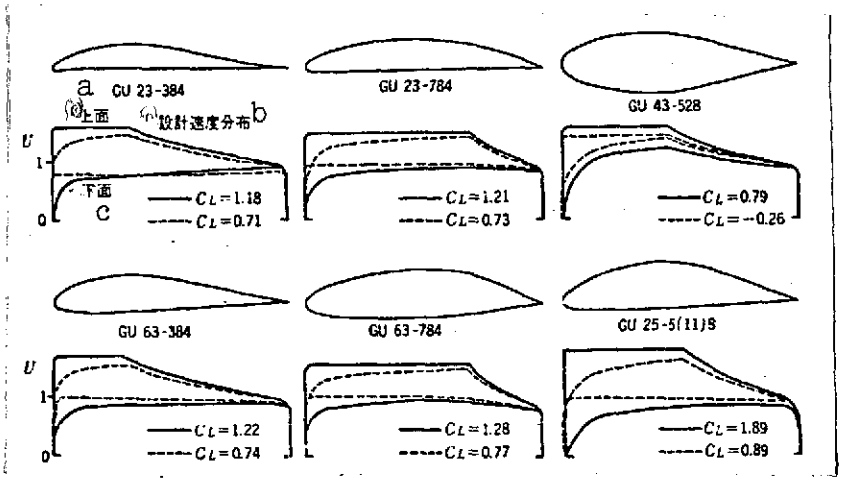

Fig. 21. Some of Nonweiler's airfoils [30].

Key: a. Upper surface
b. Design velocity distribution
c. Lower surface

In addition, Liebeck's airfoils have upper surface pressure distributions which are suitable for designing thick, separation-free struts [24] (Fig. 23).

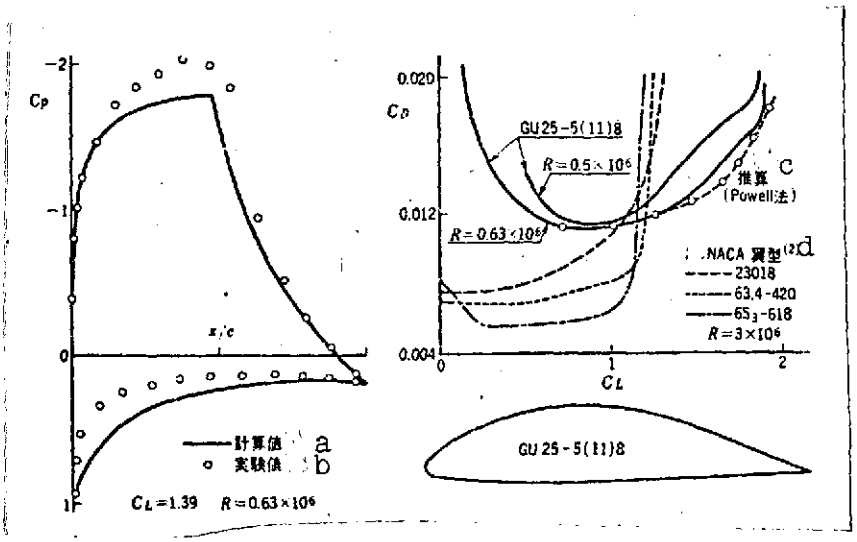

Fig. 22. Experimental results of a Nonweiler's airfoil [31].

Key: a. Calculated value
b. Experimental value
c. Estimation (Powell's method)
d. NACA airfoils [2]

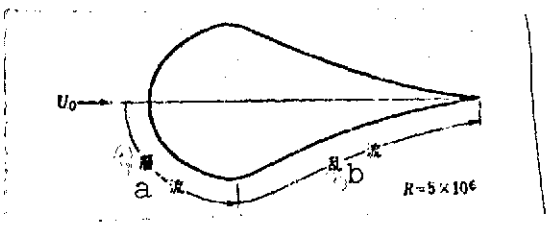

Fig. 23. Thick, separation-free strut [24].

Key: a. Laminar flow;
b. Turbulent flow

7.2. Rooftop-Rear Loading Airfoils

In the case of wings for high speed aircraft, it is required that the Mach number of rapid drag increase M_D (Fig. 7A) be high. The cause of rapid drag increase can be attributed to impact waves generated from a supersonic domain which occurs on the wing surface. The waves cause the separation of the boundary layer. The airfoils in question were designed to counter this problem. They are designed in such asway that the velocity distribution on the upper wing surface is held to below the velocity of sound at the design point (rooftop), while the insufficiency in the lift is compensated by cambering the rear part of the wing (rear loading) (Fig. 24). This airfoil type may be subjected to minor corrections

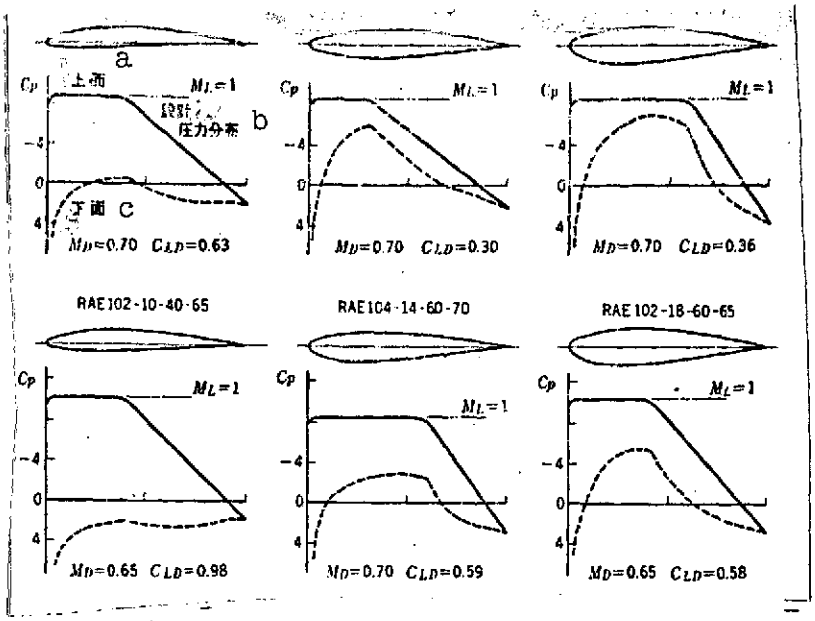

Fig. 24. Some rooftop-rear loading airfoils [32].

Key: a. Upper surface; b, Design pressure distribution; c. Lower surface

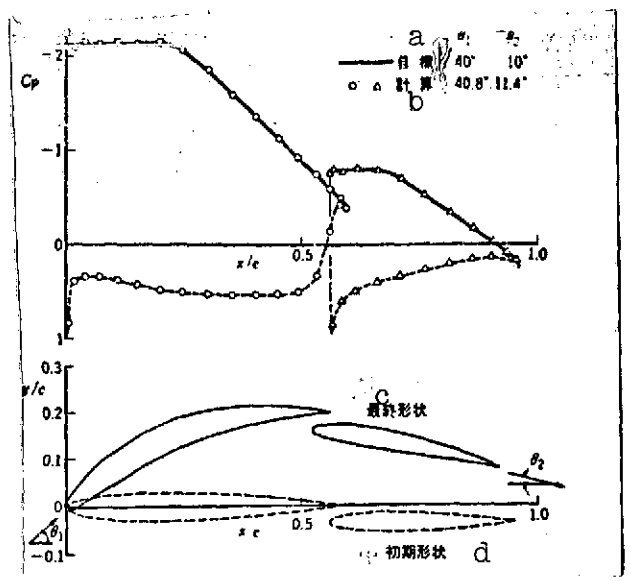

Fig. 25. Examples of tandem cascade with rooftop pressure distribution [15].

Key: a. Target; b. Calculation; c. Final profiles; d. Initial profiles.

in order to improve its characteristics outside the design point as well. Such an airfoil is used in the Europa Airbus A 300 B.

7.3. Cascade Blades

As far as cascade blades are concerned, there do not seem to be airfoils that were designed with specific objectives as were the two types mentioned above. However, the design of tandem cascades, such as the one shown in Fig. 25, has been attempted [15], so that it is conceivable that cascade blades with new profiles may be developed in the future.

8. Conclusion

Since it has become easier to design airfoils through calculation and since, at the same time, the reliability of calculations has beem improved, it is now possible to pursue the

development of airfoils, which was conducted in the past by the trial-and-error method through wind tunnel tests, in shorter periods and at lower costs. This has led to the following changes.

(1) It is now possible to develop optimal airfoils which satisfy the specifications required by new aircraft types to be developed with relative ease. This is a major improvement over the past method, which was restricted to the use of airfoils which may not have been optical from the limited selections in airfoil catalogs.

(2) The development of airfoil systems with special characteristics has become easier. In other words, various types of airfoils can be obtained by varying the velocity or pressure distribution in accordance with the target aerodynamic characteristics. In fact, the development of such airfoils, as an airfoil whose profile thickness is maximum with respect to a given drag coefficient, an airfoil whose profiles thickness is maximum for designated upper surface pressure distribution and lift coefficient, or an airfoil of high maximum lift coefficient, has been carried out.

At present, the confirmation of final characteristics still depends on wind tunnel tests, due to the insufficient accuracy of estimation of characteristics which are greatly removed from the design point. But there is a good prospect that this problem too could be handled through calculation so that it would seem that such methods as the ones discussed in this report will become indispensable in airfoil design procedures from now on.

REFERENCES

1. Riegels, F., Aerodynamische Profile [Aerodynamic Profiles], R. Ordenbourg, Munich, 1958. /11

2. Abbott, I.H. et al., Theory of Wing Sections, Dover Publications, New York, 1958.

3. Theodorsen, T. et al., "General potential theory of arbitrary wing sections," NACA TR 452, 1933.

4. Allen, J.H., "General theory of airfoil sections having arbitrary shape or pressure distribution," NACA TR 833, 1943.

5. Nitzburg, G.E. et al., "A study of flow changes associated with airfoil section drag rise at supercritical speeds," NACA TN 1813, 1949.

6. Gault, D.E., "A correlation of low-speed, airfoil-section stalling characteristics with Reynolds number and airfoil geometry," NACA TN 3963, 1967.

7. Nonweiler, T., Maximum Lift Data for Symmetrical Wings, 1955.

8. Moriya, T., "One method for obtaining the characteristics of arbitrary airfoils," Nippon kōkū gakkai dai 29 kai kōenkai zensatsu [Preprints from the 29th Lecture Meeting of the Japan Aeronautical Engineering Society], 1937. /12

9. Moriguchi, S., "Calculation methods for wing section flow velocity distributions," Nippon kōkū gakkai dai 71 kai kōenkai zensatsu [Preprints from the 71st Lecture Meeting of the Japan Aeronautical Engineering Society], 1940.

10. Eppler, R., "Results of joint application of boundary layer and profile theory," Z. Flugwiss. 8(9) (1960).

11. Spence, D.A., "The calculation of lift slopes allowing for boundary layer, with applications to the RAE 101 and 104 airfoils," ARC R & M 3137, 1958.

12. Weber, J., "The calculation of the pressure distribution on the surface of thick cambered wings and the design of wings with given pressure distribution," ARC R & M 3026, 1955.

13. Ormsbee, A.I. et al., "Multiple element airfoils optimized for maximum lift coefficient," AIAA J. 10(12) (1972).

14. Smith, A.M.O. et al., "Calculation of potential flow about arbitrary bodies," Progress in Aeronautical Sciences, Vol. 8, Pergamon Press, 1966.

15. Wilkinson, D.H., "A numerical solution of the analysis and design problems to the flow past one or more airfoils or cascades," ARC R & M 3545, 1967.

16. Wilby, P.G., "The calculation of subcritical pressure distributions on symmetric aerofoils at zero incidence," ARC CP-993, 1967.

17. Powell, B.J. et al., "The prediction of airfoil pressure distributions for subcritical viscous flows," AGARD CP-35, 1968.

18. Genetry, A.E. et al., Investigation of Aerodynamic Analysis Problems in Transonic Maneuvering, Vol. I., MDC-J 5264-01, 1971.

19. Albers, J.A., "Application of compressibility correction to calculation of inlet flow in inlet," J. Aircraft 10(7) (1973).

20. Thwaites, B., Incompressible Aerodynamics, Oxford Univ. Press, 1960.

21. Head, M.R., "Entrainment in the turbulent boundary layer," ARC R & M 3152, 1960.

22. Ishida, Y., "Method for calculation of airfoil profile drag," Nippon kōkū uchū gakkaishi [Journal of the Japan Aeronautics and Space Society] 19(213) (1971).

23. Cebeci, T. et al., "Calculation of viscous drag in incompressible flows," J. Aircraft 9(10) (1972).

24. Smith, A.M.O., "Aerodynamics of high-lift airfoil systems," AGARD CP-102, 1972.

25. Powell, B.J., "The calculation of the pressure distribution on a thick cambered airfoil at subsonic speeds including the effects of the boundary layer," ARC CP 1005, 1967.

26. Cook, T.A., "Measurements of the boundary layer and wake of two aerofoil sections at high Reynolds numbers and high subsonic Mach numbers," ARC R & M 3722, 1971.

27. Bhateley, I.C. et al., "A simplified mathematical model for the analysis of multi-element airfoils near stall," AGARD CP-102, 1972.

28. Railly, J.W., "Pure design method for airfoils in cascades," JMES 11(5) (1969).

29. Bingham, G.J., "Low-speed aerodynamic characteristics of an aerofoil optimized for maximum lift coefficient," NASA TND-7071, 1972.

30. Nonweiler, T., "A new series of low-drag aerofoils," ARC R & M 3618, 1968.

31. Kelling, E.H., "Experimental investigation of a high-lift, low-drag aerofoil," ARC CP 1187, 1969.

32. E.S.D.U., "Aerofoils having a specified form of upper-surface pressure distribution," ESD TDM-67010, 1967.

Equations for the calculation of $SC_1(\mu,\nu),\ldots,SC_5(\mu,\nu)$ [12]:

$$SC1(\mu,\nu)=\begin{cases}\dfrac{(-1)^{\mu-\nu}-1}{N}\dfrac{2\sin\frac{\mu\pi}{N}}{\left(\cos\frac{\mu\pi}{N}-\cos\frac{\nu\pi}{N}\right)^2} & \mu\neq\nu\\ \dfrac{N}{\sin\frac{\nu\pi}{N}} & \mu=\nu\end{cases}$$

$$SC2(\mu,\nu)=\begin{cases}-2\dfrac{(-1)^{\mu-\nu}\sin\frac{\mu\pi}{N}}{\sin\frac{\nu\pi}{N}\left(\cos\frac{\mu\pi}{N}-\cos\frac{\nu\pi}{N}\right)} & \mu\neq\nu\\ \dfrac{\cot\frac{\nu\pi}{N}}{\sin\frac{\nu\pi}{N}} & \mu=\nu\end{cases}$$

$$SC3(\mu,\nu)=\begin{cases}SC1(\mu,\nu)+\dfrac{2}{N}\dfrac{1-(-1)^{\mu-\nu}}{\sin\frac{\mu\pi}{N}\left(\cos\frac{\mu\pi}{N}-\cos\frac{\nu\pi}{N}\right)} & \mu\neq\nu\\ & \mu\neq N\\ \dfrac{N}{\sin\frac{\nu\pi}{N}} & \nu=\nu\end{cases}$$

$$SC4(\mu,\nu)=\begin{cases}\dfrac{(-1)^{\nu}-1}{N}\dfrac{1}{1+\cos\frac{\nu\pi}{N}} & \mu=N\\ \dfrac{2}{N}\dfrac{(-1)^{\mu-\nu}-1}{\sin\frac{\nu\pi}{N}}\dfrac{1-\cos\frac{\mu\pi}{N}\cos\frac{\nu\pi}{N}}{\left(\cos\frac{\nu\pi}{N}-\cos\frac{\mu\pi}{N}\right)^2} & \\ \quad-\dfrac{2}{N}\dfrac{(-1)^{\mu}-1}{\sin\frac{\nu\pi}{N}}\dfrac{1}{1-\cos\frac{\mu\pi}{N}} & \mu\neq\nu\\ & \mu\neq N\\ \dfrac{N}{\sin\frac{\nu\pi}{N}}-\dfrac{2}{N}\dfrac{(-1)^{\nu}-1}{\sin\frac{\nu\pi}{N}}\dfrac{1}{1-\cos\frac{\nu\pi}{N}} & \mu=\nu\end{cases}$$

$$SC5(\mu,\nu)=\begin{cases}-\dfrac{2(-1)^{\mu-\nu}}{\cos\frac{\mu\pi}{N}-\cos\frac{\nu\pi}{N}} & \mu\neq\nu\\ -\dfrac{\cot\frac{\nu\pi}{N}}{\sin\frac{\nu\pi}{N}} & \mu=\nu\end{cases}$$